Journal Name

ARTICLE

Regioselective Synthesis of Fullerene Multiadducts via Tether-directed 1,3-Dipolar Cycloaddition

Bolong Zhang, Jonathan M. White, David J. Jones and Wallace W. H. Wong*

Received 00th January 20xx,
Accepted 00th January 20xx

DOI: 10.1039/x0xx00000x

www.rsc.org/

The regioselective synthesis of fullerene multiadducts was achieved from commercially available reagents in one pot over two steps. The configuration of the isolated regioisomers was determined using various NMR methods, UV-vis spectroscopy and electrochemical analysis with the structure of one isomer confirmed by single crystal X-ray analysis. Interesting variation in regioselectivity was observed when different amino acid reagents were used in the reactions. Theoretical calculations and additional experiments, such as deuterium exchange, led to a proposed mechanism for the regioselective product formation.

Introduction

Regiochemistry of fullerenes can be complex given the large number of carbon centres that can participate in reactions.[1, 2] An effective strategy is to control the regiochemistry using a tether between two reactive head groups.[3, 4] This is known as the tether-directed remote functionalization approach which was first demonstrated by Breslow et al.[5] in mimicking highly selective enzymatic reactions on steroid compounds. This tether approach has been demonstrated in regio- and stereoselective fullerene functionalizations.[6] Tethers reported include simple arenes, porphyrins, crown ethers as well as chiral Tröger base units.[2] These previous studies investigated the scope of the tether-directed functionalization strategy but did not look into the application of the materials produced.

A central research theme in our group has been the development of organic electronic materials with particular emphasis on thin film solar cells. Bisadducts of fullerenes have been widely incorporated in solar cell devices but isomeric mixtures are commonly used. There has only been a few attempts to isolate single bisadduct isomers and investigate their performance in devices.[7, 8] In one case, a single isomer of indene-C_{70} bisadduct ($IC_{70}BA$) was obtained by careful chromatographic separation.[9] This single isomer showed significant device performance improvement compared to samples containing isomeric mixtures. However, chromatographic isolation of bisadduct isomers is extremely inefficient in terms of product yield and time required for the processing. There has been a few recent studies on the use of tether-directed functionalization to produce fullerene materials for solar cell applications.[10-12] In particular, our group has developed a one-pot synthesis of a single C_{60} bisadduct isomer from commercially available phenyl-C_{61}-butyric acid methyl ester ($PC_{61}BM$).[13] With the relatively short propyl tether and the azomethine ylide reactive head group, one major product was isolated and subsequently identified as the *cis-1* C_{60} bisadduct derivative, *N*-methyl $PC_{61}PF$ (Figure 1). This pure isomer material showed enhancement in performance compared to the isomer mixtures and the original $PC_{61}BM$ material.

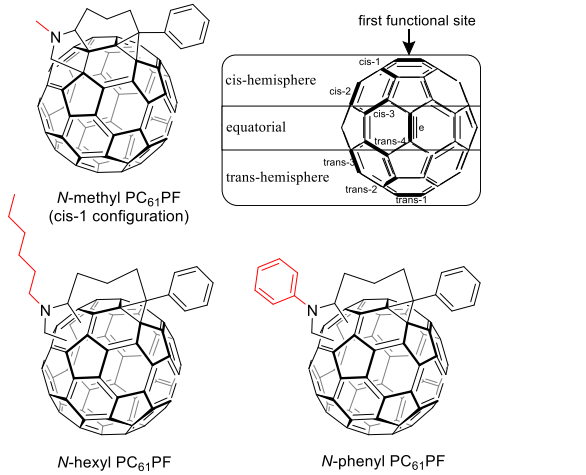

Figure 1. Chemical structure representation of bisadduct derivatives discussed in this work and an illustration of possible C_{60} bisadduct regioisomer configurations.

This positive outcome gave us incentive to develop a series of related compounds with different substitution on the pyrrolidine nitrogen (Figure 1). Interestingly, the substituent variations had significant effects on the regioselectivity of the 1,3-dipolar cycloaddition (Figure 2). Different products were isolated when *N*-hexylglycine and *N*-phenylglycine was used instead of *N*-methylglycine. In a large proportion of examples, 1,3-dipolar cycloaddition to fullerenes occurred at the [6,6] bonds, namely the C=C bonds between two six-membered rings. This can result in 8 possible regioisomers for C_{60} fullerene bisadducts (Figure 1). With the appropriate tether length, one can limit the 1,3-dipolar cycloaddition to the cis-hemisphere only. The *cis-1* configuration was the most favoured in the case

School of Chemistry, University of Melbourne Bio21 Institute, 30 Flemington Rd, Parkville, Victoria 3010, Australia. E-mail: wwhwong@unimelb.edu.au

† Electronic supplementary information (ESI) available: Details on the synthesis procedures, characterization and DFT calculations of the materials. CCDC xxxx. For ESI and crystallographic data in CIF or other electronic format see DOI: xxxxxxx

of the *N*-methyl $PC_{61}PF$ compound. Therefore, it was intriguing to observe regiochemistry variations for the *N*-hexyl and *N*-phenyl compounds even though the propyl tether was unchanged.

In this study, our efforts in the elucidation of the regioisomer configuration of the isolated products are presented. Through computations and experiments, reaction mechanisms for the product outcomes are proposed. It is noteworthy that these tether-directed reaction resulted in fused ring structures, containing 3, 5, 6 and 7-membered rings, rarely observed in the literature.

Results and Discussion

Synthesis and configuration identification

Two new C_{60} bisadducts, *N*-hexyl $PC_{61}PF$ and *N*-phenyl $PC_{61}PF$, were synthesized and fully characterized (Figure 1). As with the previously reported *N*-methyl $PC_{61}PF$, the hexyl and phenyl analogues were synthesized from $PC_{61}BM$ in a one-pot-two-step reaction (Figure 2). $PC_{61}BM$ was treated with the reducing reagent, diisobutylaluminium hydride (DIBAL), to give the aldehyde intermediate. Without isolation, the aldehyde intermediate was heated with *N*-hexylglycine or *N*-phenylglycine in 1,2-dichlorobenzene (*o*-DCB) at 180 °C to form the *N*-hexyl and *N*-phenyl $PC_{61}PF$ respectively. It was apparent immediately from thin layer chromatography analysis that the *N*-hexylglycine and *N*-phenylglycine gave different product distributions.

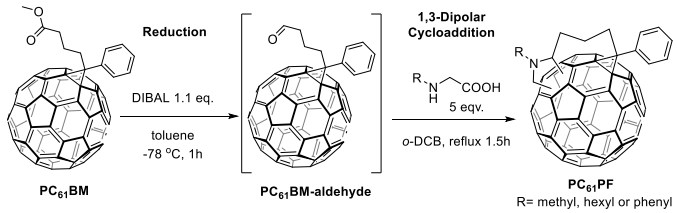

Figure 2. One-pot two-step synthesis of $PC_{61}PF$ derivatives.

The crude product of *N*-hexyl $PC_{61}PF$ was purified by silica chromatography and two major fractions were isolated, *N*-hexyl $PC_{61}PF$-1 and *N*-hexyl $PC_{61}PF$-2, in yields of 9% and 14% respectively. The purity of the two hexyl samples were examined by HPLC analysis with Cosmosil Buckyprep-D column and found to be 95% and 99% for fraction 1 and 2 respectively (Figure S22). According to the ^{1}H NMR spectrum, both fractions contained three distinct proton resonances characteristic to the pyrrolidine moiety, confirming the formation of the fulleropyrrolidine unit. However, the *N*-hexyl $PC_{61}PF$-2 fraction showed two additional singlet resonance at 5.65 and 5.45 ppm compared to *N*-hexyl $PC_{61}PF$-1. This observation corresponded to the mass spectrometry data where *N*-hexyl $PC_{61}PF$-2 was two mass units heavier than *N*-hexyl $PC_{61}PF$-1.

Full ^{1}H NMR assignment of the two fractions was achieved using two-dimensional NMR analysis techniques shown in Figure 3 and Figure 4. The heteronuclear multiple-bond correlation (HMBC) spectrum of *N*-hexyl $PC_{61}PF$-1 showed the C_{15} carbon coupled with both H_5 and H_{2b} protons (Figure 3). This coupling was observed for the *N*-methyl $PC_{61}PF$ compound with known *cis-1* regioisomer configuration. This strongly indicated *cis-1* configuration for the *N*-hexyl $PC_{61}PF$-1 fraction. With two extra proton signals, the HMBC spectrum of *N*-hexyl $PC_{61}PF$-2 was more difficult to analyse (Figure 4). There were clear HMBC coupling signals for H_{18} to C_{12} and C_{13} as well as H_{17} to C_5 and C_{14}, but no coupling with C_{15} and C_{16}. This suggested that C_{17} and C_{18} were next to C_{13} and C_{14} but not directly adjacent to C_{15} and C_{16}. In addition, H_{17} and H_{18} did not couple to each other. In light of these NMR experiments, a possible configuration of *N*-hexyl $PC_{61}PF$-2 was shown in Figure 4 with the pyrrolidine ring and the two additional protons occupied both the *cis-1* and *cis-2* position, designated as *cis-1,2* hence forth.

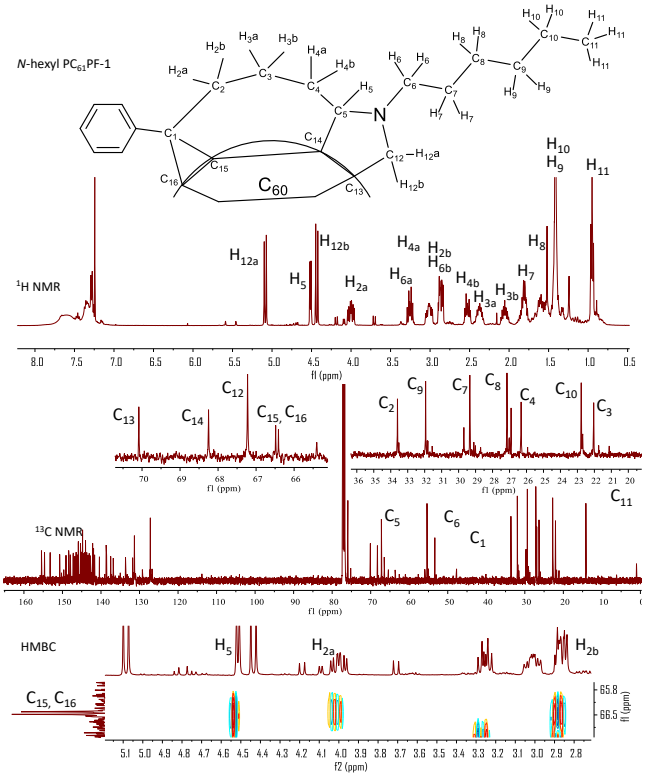

Figure 3. ^{1}H, ^{13}C and HMBC NMR spectrum of *N*-hexyl $PC_{61}PF$-1 with resonances assigned for the key atoms in discussion.

Single crystals of *N*-hexyl $PC_{61}PF$-2 were obtained by recrystallization from chloroform and subsequent X-ray crystallography experiment on the crystals revealed the relative configuration of the sample. The fused ring structure containing the pyrrolidine substituent was in agreement with the NMR assignments where the pyrrolidine ring and the two additional protons were in the *cis-1,2* configuration (Figures 4 and 5). Surprisingly, the crystallography data indicated the enantiomeric pairs in the crystal existed in a dimerized state (Figure 5). The dimerization reaction probably proceeded through a photo-activated [2+2] cycloaddition driven by the close packing in the crystal structure.[14] It is important to note that there was no evidence of the covalently linked dimer in mass spectrometry experiments prior to the crystallography analysis with the sample kept in ambient light conditions.

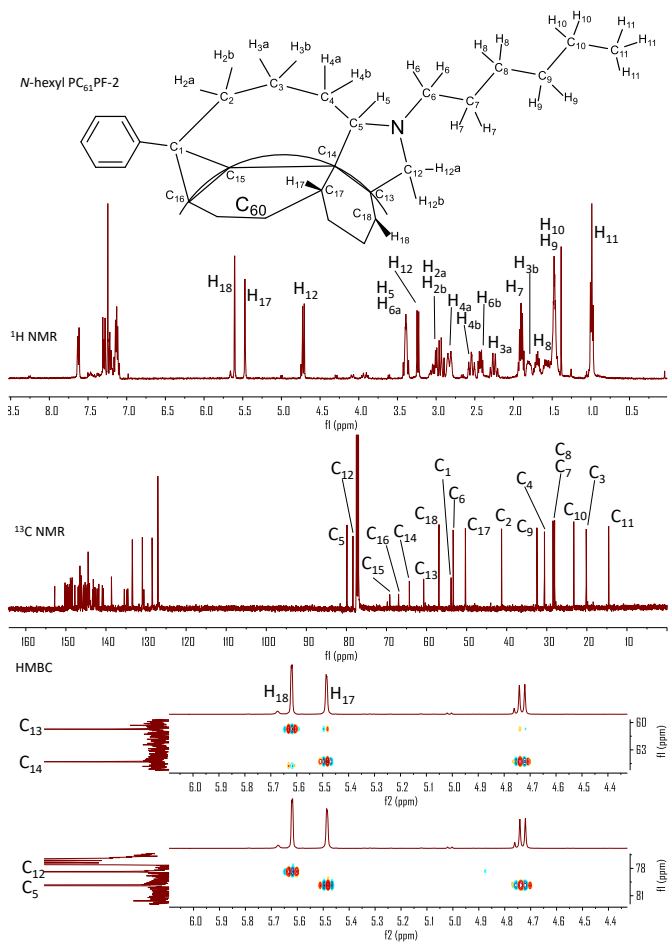

Figure 4. ^{1}H, ^{13}C and HMBC NMR spectrum of *N*-hexyl $PC_{61}PF$-2 with resonances assigned for the key atoms in discussion.

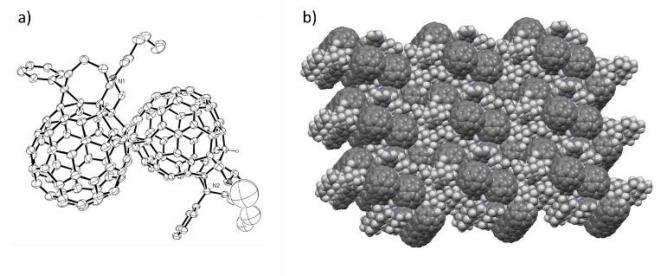

Figure 5. Single crystal X-ray structure representation of *N*-hexyl $PC_{61}PF$-2 dimer crystals grown from chloroform: a) space filling model and b) packing diagram in single crystal, where $CHCl_3$ solvent molecules have been omitted for clarity.

The crude product of *N*-phenyl $PC_{61}PF$ was purified by flash chromatography with one major fraction isolated in a yield of 14%. Some $PC_{61}BM$ stating material and aldehyde intermediate were recovered but the majority of reaction mixture consisted of insoluble material that could not be identified. The purity of the *N*-phenyl $PC_{61}PF$ sample was 77% by HPLC analysis (Figure S22). The three distinctive proton resonances of the pyrrolidine moiety were clearly observed at the chemical shift of 5.82, 5.47 and 5.35 ppm in the ^{1}H NMR spectrum. As with the hexyl compounds, key structure assignments of *N*-phenyl $PC_{61}PF$ was achieved using two-dimensional NMR analysis (Figures 6 and S13-15). Due to overlapping resonances, it was not possible to identify the regioisomer configuration for *N*-phenyl $PC_{61}PF$ in NMR experiments.

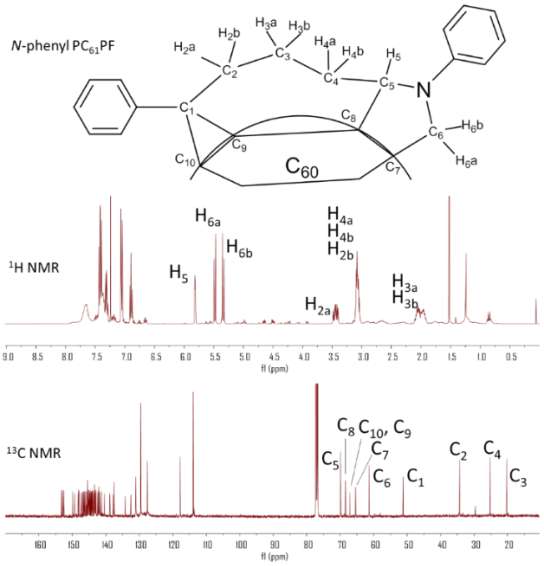

Figure 6. ^{1}H and ^{13}C spectrum of *N*-phenyl $PC_{61}PF$ with resonances assigned for the key atoms in discussion.

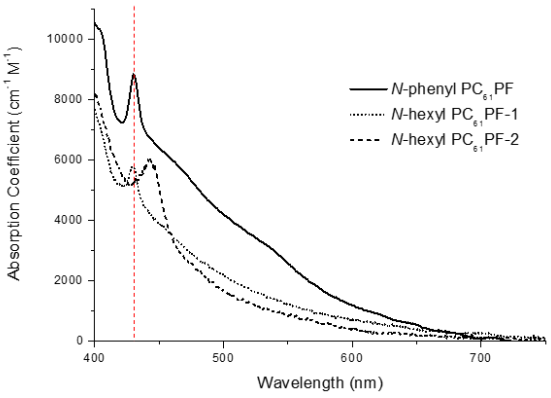

Figure 7. UV-Vis spectrum of $PC_{61}PF$ compounds.

It is well-established that the isomeric configuration of fullerene bisadducts can be identified by comparing the UV-Vis spectrum of materials with known configuration.[6] This is because the absorption bands of fullerene derivatives are closely related to the conjugated surface of the molecules. As shown in Figure 7, the spectrum of *N*-hexyl $PC_{61}PF$-1 and *N*-phenyl $PC_{61}PF$ contained a peak at 430 nm. Other C_{60} bisadducts of known *cis-1* configuration, for example *N*-methyl $PC_{61}PF$[13] and C_{60}–benzyne bisadduct[1], have similar spectral features. This provided support for the NMR analysis of the *N*-hexyl $PC_{61}PF$-1 compound and hinted at the *cis-1* configuration for *N*-phenyl $PC_{61}PF$. Notably, the UV-vis spectrum of *N*-hexyl $PC_{61}PF$-2 was different to that of *N*-hexyl $PC_{61}PF$-1 and *N*-phenyl $PC_{61}PF$ with a peak at 442 nm (Figure 7 and Table 1). Cyclic voltammetry was carried out to estimate the lowest unoccupied molecular orbital (LUMO) energy level of each $PC_{61}PF$ material (see Supporting Information for details, Figure S23). The half-wave potential of the first reduction process ($E_{1/2}^{red}$) were measured against the internal ferrocene standard and the LUMO energy can be

calculated from this data (Table 1).[15] The *N*-hexyl $PC_{61}PF$-1 sample has higher electron affinity with E_{LUMO} at -3.67 eV than *N*-hexyl $PC_{61}PF$-2 with E_{LUMO} at -3.58 eV. This corresponds to the increased substitution for *N*-hexyl $PC_{61}PF$-2. The chemical structure of the isolated regioisomers, assigned using the characterisation data, are shown in Figure 8. In the next section, calculations and discussion on the mechanism of product formation will provide support to the various characterisation techniques presented thus far.

Table 1. Summary of characterization data for $PC_{61}PF$ compounds.

	Purity (%) [a]	configuration	UV-vis λ_{max} (nm) [b]	$E_{1/2}^{red}$ (eV) [c]	E_{LUMO} (eV) [d]
N-hexyl $PC_{61}PF$-1	95	*cis-1*	430 (5.8)	-1.13	-3.67
N-hexyl $PC_{61}PF$-2	99	*cis-1,2*	442 (6.0)	-1.22	-3.58
N-phenyl $PC_{61}PF$	77	*cis-1*	431 (8.8)	-1.25	-3.55

[a] Calculated by HPLC analysis; [b] Absorption coefficient ($\times 10^3$ $M^{-1}cm^{-1}$) in brackets; [c] Half-wave reduction potential from cyclic voltammetry; [d] E_{LUMO} = -($E_{1/2}^{red}$ + 4.8) eV.

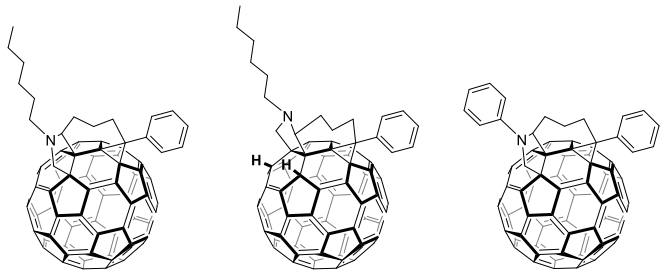

N-hexyl $PC_{61}PF$-1 *N*-hexyl $PC_{61}PF$-2 *N*-phenyl $PC_{61}PF$

Figure 8. Chemical structures of *N*-hexyl $PC_{61}PF$-1, *N*-hexyl $PC_{61}PF$-2 and *N*-phenyl $PC_{61}PF$

Density functional theory (DFT) calculations

The unusual *cis-1,2* configuration for *N*-hexyl $PC_{61}PF$-2 was examined in DFT calculations to support our experimental observations. The proposed reaction pathway leading to the observed products is discussed below (Figure 9). One can consider the azomethine ylide as the starting point of discussions. For *N*-hexyl $PC_{61}PF$-1 and *N*-phenyl $PC_{61}PF$, the *cis-1* product can be formed by 1,3-dipolar cycloaddition in one step. On the other hand, the insertion of two additional protons for *N*-hexyl $PC_{61}PF$-2 with *cis-1,2* configuration probably involved at least two steps. In detail, the 1,3-dipolar cycloaddition proceeded first to form the pyrrolidine ring on the [5,6] bond followed by protonation to give the *cis-1,2* product. Therefore, there must be an intermediate between the transition state of the cycloaddition step and the transition state of the protonation step. Using this model and applying DFT at B3LYP-D3 level[16, 17] with 6-311G basis set and polarization function (d,p), the relative energy of the azomethine ylide starting point, transition states, possible intermediates and final products were calculated (Figure 10 and Table S1).[18, 19]

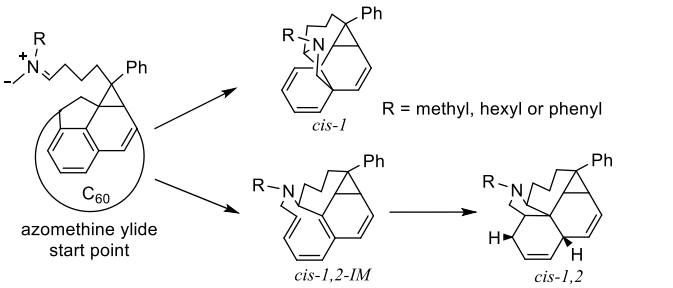

Figure 9. Proposed reaction pathway for $PC_{61}PF$ products with cis-1 and cis-1,2 configuration.

Since the product energy of $PC_{61}PF$s in *cis-1,2* configuration were much lower than both the intermediates *cis-1,2-IM*[20, 21] and the products of *cis-1*, the formation of the *cis-1,2* product can be considered as irreversible (Figure 10). On the other hand, an equilibrium may exist between *cis-1* and *cis-1,2-IM* species. From the calculated Gibbs free energy difference (ΔΔG) values between *cis-1* and *cis-1,2-IM*, relative equilibrium constant (K) values can be obtained using the equations:

$$K = e^{\frac{(-\Delta\Delta G)}{RT}} \quad (1)$$

$$K = \frac{[cis{-}1,2{-}\mathrm{IM}]}{[cis{-}1]} \quad (2)$$

where *R* is the gas constant and *T* is the reaction temperature. With $\Delta\Delta G_1$ of *N*-methyl $PC_{61}PF$ larger than $\Delta\Delta G_2$ of *N*-hexyl $PC_{61}PF$ (Figure 10), the corresponding K for the methyl species was much smaller ($K_1 = 4.1 \times 10^{-9}$) than the hexyl species ($K_2 = 8.9 \times 10^{-4}$). The consequence of this difference was that a much greater proportion of the hexyl species would exist in the *cis-1,2-IM* form compared to the methyl at equilibrium, leading to a greater chance of formation of the *cis-1,2* product for the hexyl. This corresponded to the *N*-hexyl $PC_{61}PF$-1 and *N*-hexyl $PC_{61}PF$-2 compounds that were isolated. A steric argument can be invoked for the outcome of the calculated ΔΔG values. The significantly higher energy of the hexyl *cis-1* species can be attributed to the steric bulk of the hexyl group compared to the methyl group (Figure S26). The steric effect of the hexyl moiety in *cis-1,2-IM* configuration was not as significant resulting in similar energies for the hexyl and methyl *cis-1,2-IM* species.

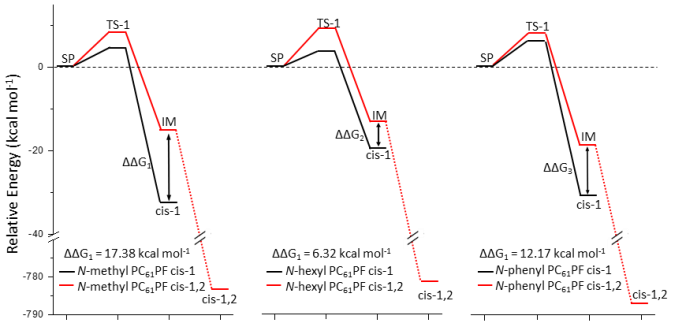

Figure 10. Relative energy of starting point, transition states, intermediates and products of $PC_{61}PF$ compounds with cis-1 and cis-1,2 configuration from DFT calculations.

Although the phenyl group should have stronger steric effect than hexyl, *cis-1,2* product was not observed for *N*-phenyl $PC_{61}PF$. The DFT calculation revealed a relatively large $\Delta\Delta G_3$ for the phenyl compounds (Figure 10). This meant that only a small

concentration of *cis-1,2-IM* of *N*-phenyl $PC_{61}PF$ existed at equilibrium (K_3 = 1.3 × 10^{-6}), resulting in less *cis-1,2* product compared to hexyl species. A possible reason could be that the phenyl group was able to stablize the *cis-1* product by sharing the electron density with the pyrrolidine moiety. According to the DFT optimized molecular models, the orientation of the phenyl ring relative to the pyrrolidine ring was very different for the *cis-1* and *cis-1,2-IM* species. Only the optimised geometry of *cis-1* showed electronic stabilization effect of the phenyl group. In the *cis-1,2-IM* species, steric hinderance between the phenyl group and the H_4 proton resulted in an orientation of the phenyl ring relative to the pyrrolidine ring that did not favor electronic stabilization (Figure S27).

Deuterium exchange experiments and proposed mechanism

To gain further insight into the reaction mechanism, deuterium exchange experiments were performed. The reactions to form the hexyl compounds were carried out as before except with the addition of deuterium oxide in the reaction mixture of the 1,3-dipolar cycloaddition step (see Experimental Section for details). The ^{1}H NMR spectrum showed that deuterium exchange occurred at two protons (H_{4a} and H_{4b}) in *N*-hexyl $PC_{61}PF$-1 and four (H_{4a}, H_{4b}, H_{17} and H_{18}) in *N*-hexyl $PC_{61}PF$-2 (Figure S16 and S17). The exchanges at the H_{4a} and H_{4b} proton could be simply attributed to the keto-enol tautomerisation of the aldehyde starting material. The deuterium exchange at H_{17} and H_{18} for the *N*-hexyl $PC_{61}PF$-2 material provided information on the source of those protons (Figure 11). It was noteworthy that the percentage of deuterium exchange at H_{15} and H_{18} were both around 80% by integration. The following is a descirption of the proposed reaction mechanism for the formation of the *cis-1* and *cis-1,2* products taking into account all experimental data and calculations.

The mechanism of formation of the *cis-1* product proceeded via 1,3-dipolar cycloaddition of azomethine ylide to *cis-1* bond of the C_{60} derivative (Figure 11). This reaction, known as the Prato reation, is commonly observed in the literature but usually proceeds without regioselectivity.[22, 23] In order to achieve the *cis-1,2* product outcome, the 1,3-dipolar cycloaddition would be required to occur at the [5,6] bond between the *cis-1* and *cis-2* positions (Figure 11).[20, 21] This open cage intermediate *cis-1,2-IM* would then be converted to the close cage intermediate via a hydride transfer reaction. Further protonation would lead to the *cis-1,2* product. It is feasible that the hydride source is from the fullerene aldehyde substrate leading to a fullerene amide by-product. This proposal is in agreement with the observed product yields. A reaction with deuterated DIBAL reagent was performed in an attempt to gather further evidence for the proposed mechanism (see Suppoting Information, Figure S18). In agreement with the azomethine ylide formation mechanism, the H_5 proton on the pyrrolidine ring was deuterated. However, deuteration was not observed for either the H_{17} or H_{18} on the fullerene surface. It was found that the acidity of H_{17} and H_{18} was such that there was facile proton exchange under the reaction conditions (Figure S19). Attempts were made to identify intermediates and by-products from the reaction mixture using mass spectrometry. While some relevant fragments were observed, these experiments did not provide conclusive evidence for the proposed reaction mechanism.

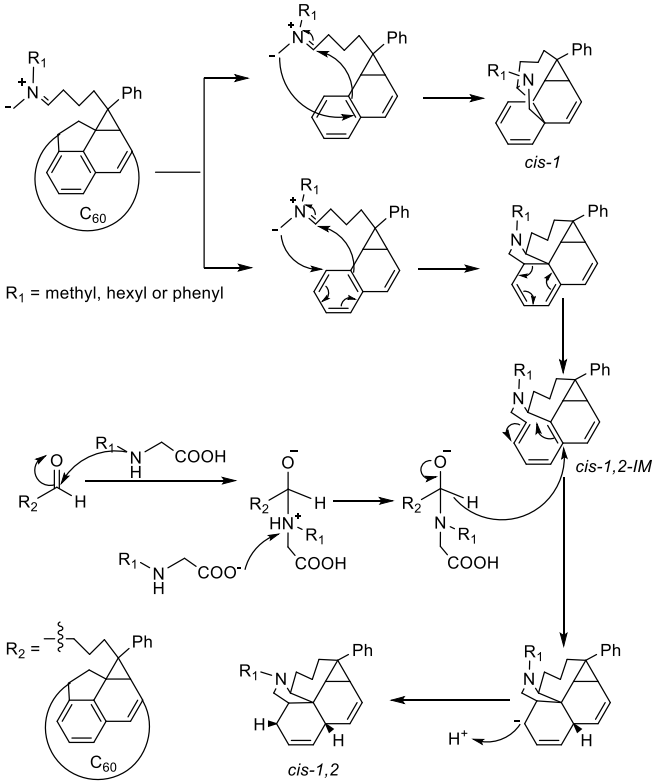

Figure 11. The proposed mechanism for the formation of $PC_{61}PF$ compounds in either cis-1 or cis-1,2 configuration.

Conclusions

The regioselective synthesis of three fullerene derivatives was presented. Starting from commercially available $PC_{61}BM$, the multi-adducts were obtained via reduction of the methyl ester followed by 1,3-dipolar cycloaddition of the azomethine ylide in one pot. While the yields were moderate, intriguing regioselectivity variations were observed when different amino acid reagents were used. With a range of NMR methods, UV-Vis spectroscopy and electrochemical analysis, it was possible to confidently assign the configurations of the isolated regioisomers *N*-hexyl $PC_{61}PF$-1 (*cis-1*), *N*-hexyl $PC_{61}PF$-2 *(cis-1,2*) and *N*-phenyl $PC_{61}PF$ (*cis-1*). The relative configurations for *N*-hexyl $PC_{61}PF$-2 was confirmed by single crystal X-ray analysis. Mechanism for the product formation was proposed with the aid of DFT calculations and deuterium exchange experiments.

Acknowledgements

This work was made possible by support from the Australian Renewable Energy Agency which funds the project grants within the Australian Centre for Advanced Photovoltaics. WWHW is supported by an Australian Research Council Future Fellowship (FT130100500). Responsibility for the views, information, or

advice herein is not accepted by the Australian Government. We thank Dr. Lars Goerigk for providing advice on the DFT calculations.

Notes and references

Detailed experimental procedures, NMR spectra and other characterization data as well as details on the modelling and theoretical calculations can be found in the Supporting Information.

1. Y. Nakamura, N. Takano, T. Nishimura, E. Yashima, M. Sato, T. Kudo and J. Nishimura, *Org. Lett.*, 2001, **3**, 1193-1196.
2. C. Thilgen and F. Diederich, *C. R. Chim.*, 2006, **9**, 868-880.
3. M. R. Cerón, M. Izquierdo, A. Aghabali, J. A. Valdez, K. B. Ghiassi, M. M. Olmstead, A. L. Balch, F. Wudl and L. Echegoyen, *J. Am. Chem. Soc.*, 2015, **137**, 7502-7508.
4. L. Isaacs, R. F. Haldimann and F. Diederich, *Angew. Chem. Int. Ed.*, 1994, **33**, 2339-2342.
5. R. Breslow, *Acc. Chem. Res.*, 1980, **13**, 170-177.
6. W. W. H. Wong and F. Diederich, *Chem. Eur. J.*, 2006, **12**, 3463-3471.
7. X. Meng, G. Zhao, Q. Xu, Z. a. Tan, Z. Zhang, L. Jiang, C. Shu, C. Wang and Y. Li, *Adv. Funct. Mater,*, 2014, **24**, 158-163.
8. F. Zhao, X. Meng, Y. Feng, Z. Jin, Q. Zhou, H. Li, L. Jiang, J. Wang, Y. Li and C. Wang, *J. Mater. Chem. A*, 2015, **3**, 14991-14995.
9. W. W. H. Wong, J. Subbiah, J. M. White, H. Seyler, B. Zhang, D. J. Jones and A. B. Holmes, *Chem. Mater.*, 2014, **26**, 1686-1689.
10. M.-H. Liao, Y.-Y. Lai, Y.-Y. Lai, Y.-T. Chen, C.-E. Tsai, W.-W. Liang and Y.-J. Cheng, *ACS Appl. Mater. Interfaces*, 2014, **6**, 996-1004.
11. R. Tao, T. Umeyama, T. Higashino, T. Koganezawa and H. Imahori, *Chem. Commun.*, 2015, **51**, 8233-8236.
12. R. Tao, T. Umeyama, T. Higashino, T. Koganezawa and H. Imahori, *ACS Appl. Mater. Interfaces*, 2015, DOI: 10.1021/acsami.5b04351.
13. B. Zhang, J. Subbiah, Y. Y. Lai, J. M. White, D. J. Jones and W. W. Wong, *Chem. Commun.*, 2015, **51**, 9837-9840.
14. G.-W. Wang, K. Komatsu, Y. Murata and M. Shiro, *Nature*, 1997, **387**, 583-586.
15. C. M. Cardona, W. Li, A. E. Kaifer, D. Stockdale and G. C. Bazan, *Adv. Mater.*, 2011, **23**, 2367-2371.
16. S. Grimme, J. Antony, S. Ehrlich and H. Krieg, *J. Chem. Phys.*, 2010, **132**, 154104.
17. S. Grimme, S. Ehrlich and L. Goerigk, *J. Comput. Chem.*, 2011, **32**, 1456-1465.
18. S. Osuna, M. Swart and M. Sola, *J. Phys. Chem. A*, 2011, **115**, 3491-3496.
19. J.-C. Brodovitch, B. Addison-Jones, K. Ghandi, I. McKenzie and P. W. Percival, *Phys. Chem. Chem. Phys.*, 2015, **17**, 1755-1762.
20. Z. Li and P. B. Shevlin, *J. Am. Chem. Soc.*, 1997, **119**, 1149-1150.
21. T. Grösser, M. Prato, V. Lucchini, A. Hirsch and F. Wudl, *Angew. Chem. Int. Ed.*, 1995, **34**, 1343-1345.
22. M. Prato and M. Maggini, *Acc. Chem. Res.*, 1998, **31**, 519-526.
23. M. Maggini, G. Scorrano and M. Prato, *J. Am. Chem. Soc.*, 1993, **115**, 9798-9799.